

Depinning and critical-current characteristics of topologically defected vortex lattices

Paolo Moretti and M.-Carmen Miguel

Departament de Física Fonamental, Facultat de Física, Universitat de Barcelona, Av. Diagonal 647, E-08028 Barcelona, Spain

(Received 21 November 2008; revised manuscript received 2 February 2009; published 9 March 2009)

We discuss the role of dislocation assemblies such as grain boundaries in the dynamic response of a driven vortex lattice. We simulate the depinning of a field-cooled vortex polycrystal and observe a general enhancement of the critical current as well as a distinct crossover in the characteristic of this quantity as a function of pinning density. The results agree with analytical predictions for grain-boundary depinning. The dynamics of grain boundaries thus proves an essential mechanism underlying the flow response of defected vortex lattices and the corresponding transport properties of the superconducting material. We emphasize the connection between the topological rearrangements of the lattice and its threshold dynamics. Our theory encompasses a variety of experimental observations in vortex matter as well as in colloidal crystals.

DOI: [10.1103/PhysRevB.79.104505](https://doi.org/10.1103/PhysRevB.79.104505)

PACS number(s): 74.25.Qt, 61.72.Lk, 61.72.Mm, 74.25.Sv

The possibility of tuning mechanical properties of vortex lattices in type II superconductors has made of vortex physics a versatile framework to study several central problems of condensed-matter flow.¹ One of the most intriguing experimental features of vortex dynamics in disordered samples is the emergence of memory effects. Hysteresis of the I - V curve is often encountered when driving defected vortex lattices above and below their depinning threshold in both low T_c superconductors, such as NbSe₂ (Refs. 2–4) and high- T_c anisotropic superconductors, such as B₂Sr₂CaCu₂O₈.⁵ Numerical evidence of hysteretic behavior has also been collected, by simulating driven vortex dynamics in the presence of quenched disorder. The system was initially “prepared” in a disordered state by letting it relax from a high-temperature liquidlike phase, according to what is known as a *field-cooling* protocol in experiments.⁶ Afterward currents were ramped up and down and two distinct branches could be found in the I - V characteristic. The emergence of hysteresis indeed represents a shattering evidence of plastic flow in driven lattices. The voltage recorded in experiments is a direct measure of collective velocity of the vortex ensemble, while the applied currents act on vortices as an external driving force through a Lorentz-type coupling.¹ An I - V measurement is thus an experimental visualization of the force vs velocity relation in a driven overdamped medium. The elastic theory of transport in such systems, the well-known elastic depinning theory, does not account for history dependence in force-velocity relations.⁷ Such beyond-elastic features suggest the appearance of plastic phenomena and their involvement in memory effects. The critical current of the defected vortex array is thus a plastic threshold to vortex motion, which is found to depend on the history of the sample. Several experimental studies of the critical current J_c of vortex lattices have been carried out through the past decades. They include measurements of J_c as a function of both the applied magnetic field H (Refs. 2 and 8) and the temperature.⁹ In all systems, as a field-cooled (FC) vortex assembly is driven by a dc or pulsed signal, it behaves as if it was driven out of a metastable state through an annealing process, so that the critical current of the annealed sample proves lower than that of the initial field-cooled configuration. Such a process is governed by a current-dependent annealing time, which diverges as the critical current is ap-

proached from above.² In fact it was shown that in the presence of surface barriers at the edge of a sample, the field-cooled and the annealed phases can even coexist, as a result of the balance between bulk currents, which drive the annealing process, and edge currents, which produce contamination effects.^{10,11} It is now widely accepted that such a nonannealed field-cooled state should correspond to a peculiar topological rearrangement of the vortex array, namely, a disordered phase. This is in agreement with the experimental observation of glassy features such as power-law distributed relaxation times.² High-drive annealing is thus a process by which the vortex assembly recovers its topological order. The correspondence between topological disorder and higher critical currents is ubiquitous in such systems, another example being the phenomenology of the so-called *peak effect*. In that case a critical-current jump accompanies a disordering transition at high temperature or field. In field-cooling experiments, instead, one focuses on the metastable low-field and low-temperature state originated after a rapid temperature quench.

As for the nature of the field-cooled phase, Delaunay triangulation patterns suggest that the topological order of the vortex lattice is broken by edge dislocations, which tend to arrange themselves into linear arrays such as grain boundaries (GBs). The vortex array is thus frozen in a polycrystalline state. Vortex polycrystals have been observed, after field cooling, in various superconducting materials such as NbMo,^{12,13} NbSe₂,^{14–17} BSSCO,¹⁸ and YBCO.¹⁹

In this paper, we address the problem of plastic depinning of such systems. We simulate driven vortex polycrystals and demonstrate that for weak pinning forces, the threshold behavior observed in field-cooled samples agrees with our analytical predictions based on mechanisms of grain-boundary depinning. We are able to establish a tight connection between the topology of the vortex polycrystal and its electro-dynamical response. This correspondence was first suggested in early numerical studies.^{20,21} Our aim is to determine how the current response of these systems is affected by tuning crucial parameters such as the defect density N_p and the magnetic field (proportional to the number of vortices N_v), and to emphasize how the topology of the vortex ensemble reflects these changes. Transport properties in our simulations are quantified by looking at the critical current J_c of the

vortex array and the vortex velocity field at depinning.

Simulations are performed for a two-dimensional (2D) superconducting cross section of linear size $L=36\lambda$ (Ref. 22) with periodic boundary conditions. Here λ is the London penetration depth and all lengths are expressed in units of λ . In particular, we choose a value of $\xi=0.2\lambda$ for the coherence length (Ginzburg-Landau parameter $\kappa=5$, as found, e.g., in low- T_c superconducting alloys). The dynamics of each vortex i at position \mathbf{r}_i is described by Langevin equations of motion of the form

$$\Gamma d\mathbf{r}_i/dt = \sum_j \mathbf{f}_{vv}(\mathbf{r}_i - \mathbf{r}_j) + \sum_j \mathbf{f}_{vp}(\mathbf{r}_i - \mathbf{r}_j^p) + \mathbf{f}_L(\mathbf{r}_i), \quad (1)$$

where Γ is an effective viscosity for vortex flow. The first term on the right-hand side of such equations captures the physics of vortex mutual interactions via the long-range force,

$$\mathbf{f}_{vv}(\mathbf{r}) = AK_1\left(\frac{|\mathbf{r}|}{\lambda}\right)\hat{r}, \quad (2)$$

where $A=\Phi_0^2/(8\pi^2\lambda^3)$, Φ_0 is the quantized flux carried by the vortices, and K_1 is a first-order modified Bessel function.²³ The second contribution introduces the attraction exerted by each of the N_p point defects on vortices. Point defects are randomly located at positions \mathbf{r}_i^p ($i=1, \dots, N_p$) within the simulation box and reproduce the effect of oxygen vacancies or other impurities in the material. They exert pinning forces according to a Gaussian potential of the form

$$V(\mathbf{r} - \mathbf{r}^p) = V_0 \exp\left[-\left(\frac{\mathbf{r} - \mathbf{r}^p}{\xi}\right)^2\right], \quad (3)$$

whose amplitude and standard deviation are V_0 and ξ , respectively. If an external current $\mathbf{J}(\mathbf{r})$ is eventually applied to the sample, it generates a Lorentz-type force acting on the vortices,

$$\mathbf{f}_L(\mathbf{r}) = \frac{\Phi_0}{c} \mathbf{J}(\mathbf{r}) \times \hat{z}, \quad (4)$$

where c is the speed of light. The coupled equations of motion [Eq. (1)] are numerically solved with an adaptive step-size fifth-order Runge-Kutta algorithm, imposing periodic boundary conditions in both directions.

Field-cooled configurations are obtained by letting a random vortex array relax in the impure environment and in the absence of external forces. The system relaxes into a vortex polycrystal, in agreement with experimental evidence.

We expect the number of defects N_p to affect the relaxation process. As a matter of fact, defects are responsible for the polycrystalline order observed after relaxation. Vortex mutual interactions try to restore lattice order; however, defects hinder this process. While varying the number of pinning centers N_p , we observed that all relaxed systems exhibit grain structure. Typical grain sizes are found to decrease rapidly while increasing N_p for low impurity densities. For higher impurity densities, instead, the decrease in grain size becomes slower upon increasing N_p . At very high N_p , grain structures become extremely complex and any further decrease in grain size becomes hard to detect. Figures 1(a) and

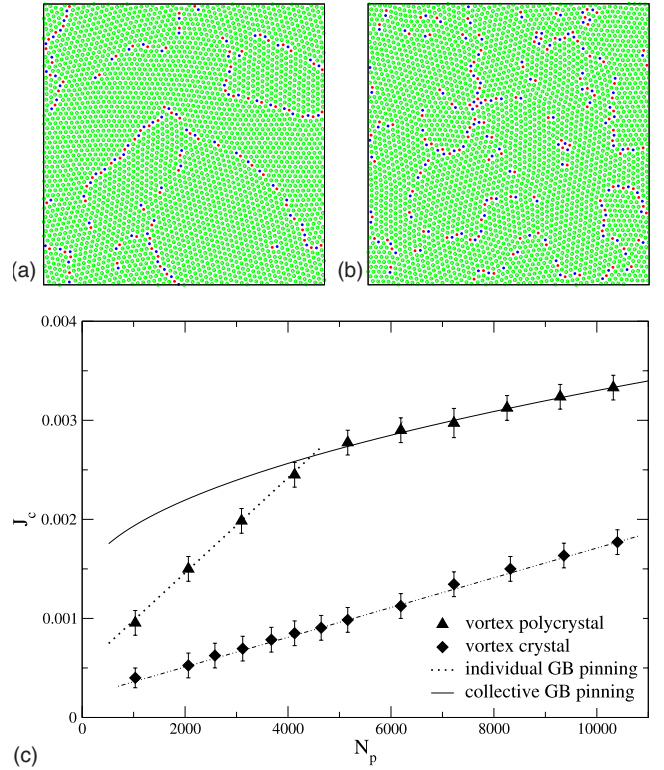


FIG. 1. (Color online) (a) Grain structure of the relaxed state for low pinning densities ($N_p=1032$) and (b) for high pinning densities ($N_p=8256$). Dislocations are identified as pairs of seven- and five-coordinated vortices (filled circles, blue and red, respectively) (c) Critical current of the field-cooled vortex array as a function of the number of quenched impurities, as obtained for a vortex polycrystal (triangles) and a vortex single crystal (diamonds), for $N_v=3120$ vortices. Numerical results are compared to the theoretical predictions for individual GB pinning (dotted line) and collective GB pinning (solid line) (see text for both cases). The straight line joining vortex-crystal points (dash-dotted) is drawn as a guide to the eyes (Ref. 24).

1(b) display typical vortex array topologies in both regimes of low and high impurity density.

We found that this behavior shows a natural correspondence with critical currents. Starting from the above relaxed configurations, we determine critical currents, as reported in Fig. 1(c). As expected, we see critical currents increase with increasing defect densities. At the same time, we observe that where we previously spotted a qualitative change in the grain size decrease, a crossover from a linear to a slower increase in critical currents appears. Similar behavior is obtained for different vortex densities. Indeed, Fig. 2 shows the same critical-current traits for simulations with different numbers of vortices in the system $N_v=1020, 2016,$ and 3120 .

In order to understand this correspondence, we have to focus on how grain structure might affect depinning of the vortex assembly. Compared to a perfect lattice, a polycrystal is a system with a much larger number of degrees of freedom, coming from the countless ways dislocations and grain boundaries can cooperatively move and rearrange. As a consequence, a vortex polycrystal will find it easier to adjust to disorder than a perfect lattice or even than a less defected

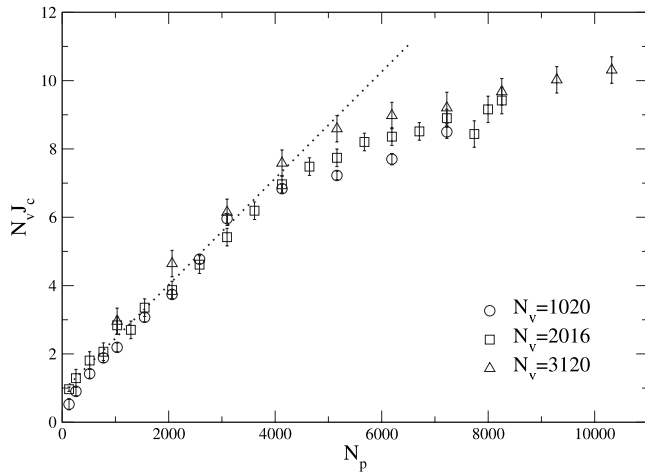


FIG. 2. Rescaled critical current as a function of the number of defects for three different vortex densities. The cases of $N_v=1020$, 2016, and 3120 vortices are depicted. Numerical data collapse where an individual GB-pinning description holds, while they deviate as soon as collective GB-pinning mechanisms take over. The dotted line is drawn as a guide to the eyes.

polycrystal. A better adjustment to disorder means in general a higher depinning threshold and eventually a higher critical current. Then it is no coincidence that critical currents increase *rapidly* (linearly) in the region where grain sizes decrease and slow down where no further grain size decrease can be discerned.

At this point, one might wonder what the behavior of a perfect crystal would be under the same conditions. A perfect crystal relaxes in the presence of weak disorder into the well-known Bragg glass phase, which retains triangular lattice ordering over accessible length scales.²⁵ Such an experimental protocol is known as zero-field cooling (ZFC). We simulated ZFC lattices and measured critical currents as we did for their FC polycrystalline counterparts. Results for the case of $N_v=3120$ are also shown in Fig. 1(c) for comparison. Two main observations can be made: (i) as discussed above and confirmed by experiments,^{2-4,8} critical currents are higher for a vortex polycrystal; and (ii) no crossover behavior is observed for a vortex crystal as the number of pinning points N_p is increased. The latter observation represents a crucial result of our work. The dynamic response of a vortex polycrystal proves radically different from that of a dislocation-free lattice. The presence of dislocation assemblies such as grain boundaries seems to affect the depinning of the vortex array in dramatic fashion.

We found that close to depinning the dynamics are highly heterogeneous (see Fig. 3). Several swirls appear and disappear intermittently in the vortex velocity field and produce significant transversal excursions. By superimposing vortex velocity fields and the corresponding topological arrangements (Fig. 4) and monitoring the time evolution of the system, we can conclude that vortex motion is activated exclusively around depinned grain boundaries and complicated velocity patterns emerge in response to GB and dislocation motion. Such regions show higher mobility and large transversal deviations. On the contrary, dislocation-free regions remain dynamically frozen, unless forces well above the de-

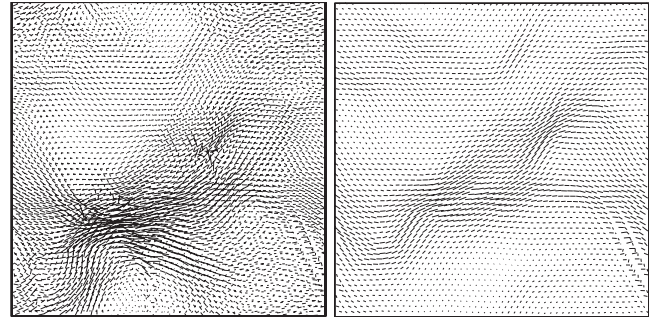


FIG. 3. Velocity fields at incipient depinning for a FC polycrystal (left) and a ZFC perfect lattice (right). Plastic depinning and dislocation dynamics are signaled by the emergence of heterogeneity and convective vortex rearrangements. In a perfect vortex lattice, instead, elastic depinning is accompanied by widespread avalanches.

pinning threshold are applied. Heterogeneity and coexistence of pinned and moving regions are indeed observed experimentally in vortex matter²⁶ as well as in colloidal polycrystals.²⁷

Such observations corroborate the idea that grain boundaries and possibly dislocation assemblies in general are crucial in the depinning transition of vortex polycrystals. As a consequence, we propose that the threshold mechanisms of a driven vortex polycrystal should be governed by grain-boundary depinning. In three recent publications of ours we proposed a theory of GB depinning.^{6,28,29} A central quantity in a depinning theory is indeed the critical force. Our system is effectively a quasi-two-dimensional lattice, where translational invariance is assumed along the direction of the field, as in thin superconducting films. Hence the critical force is defined per unit length and reads $b\sigma_c$, σ_c being the critical stress that produces GB depinning.

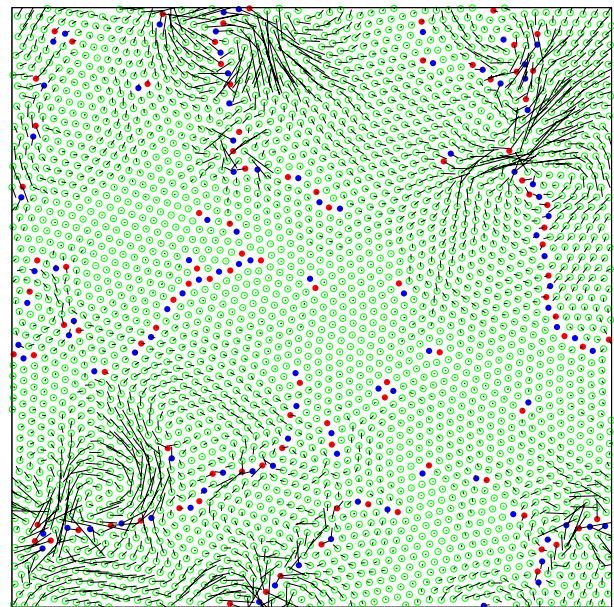


FIG. 4. (Color online) Velocity fields at incipient depinning for a FC polycrystal. The grain structure is highlighted. Vortex motion is nucleated exclusively around depinning grain boundaries.

For high defect concentrations, the vortex lattice is collectively deformed by the superposition of strain fields produced by defects. The straining of the vortex lattice results in a collective stress field acting on vortex lattice dislocations and grain boundaries as an effective pinning field. We refer to this regime as collective GB pinning. In our two-dimensional system, the critical stress σ_c can be calculated as follows: deforming a GB segment of length L of an amount u is associated with an energy cost (per unit length),

$$\mathcal{E} = K \frac{b^2}{D^2} u^2 - K \frac{ab}{D} u \left(\frac{L}{R_a} \right)^{1/5} + \frac{b}{D} \sigma L u, \quad (5)$$

where K is the shear modulus of the vortex polycrystal, a is the vortex lattice constant, D is the average dislocation spacing within the GB, and b is the modulus of the dislocation Burgers vector. Here R_a is defined as the collective pinning length of a quasi-two-dimensional vortex lattice.²⁰ The first term in Eq. (5) quantifies the elastic deformation energy due to the small displacement u . It accounts for the properties of nonlocal elasticity of deforming grain boundaries in two dimensions and its derivation was first obtained in Ref. 6. The second term is the energy gain associated with the same deformation and due to the presence of pinning points. It is derived here for two dimensions, following the same method described in Refs. 6 and 29 for a three-dimensional system. Finally, the third term in Eq. (5) is the work done by an external stress σ in displacing the boundary segment over a distance u . As described in Ref. 29 for the three-dimensional case, minimizing the first two terms with $u \approx a \approx b$ one obtains the GB-pinning length $L_p = (b/D)^5 R_a$. The critical stress σ_c is then derived as the stress required to depin a segment of length L_p and reads

$$b \sigma_c^{\text{coll}} = K \frac{D^4}{b^2} \frac{1}{R_a}. \quad (6)$$

As mentioned above, R_a is the collective pinning length of a 2D vortex lattice, and its expression is given by

$$R_a = \frac{c_{66}}{f_0 (n_p n_v)^{1/2}}, \quad (7)$$

where f_0 is the typical pinning strength acting on the lattice, n_p is the defect density, strictly proportional to N_p , n_v is the vortex density, while c_{66} is the shear modulus of the vortex lattice. Under such conditions of high pinning density, we already pointed out that the vortex lattice is highly defected and one has to assume that in principle $K \neq c_{66}$.

For low defect concentrations, instead, pinning is not mediated by the lattice and grain-boundary dislocations are individually pinned by impurities. Hence the individual GB depinning stress σ_c for a two-dimensional system reads

$$b \sigma_c^{\text{ind}} = \frac{1}{K'} \left(\frac{D}{b} \right)^2 f_0^2 n_p, \quad (8)$$

as derived in Ref. 29, where the two-dimensional model proved effective in describing systems with columnar disorder. K' is the shear modulus of the vortex polycrystal for low pinning concentrations. Under such conditions, the vortex lattice is split in very large grains and one can assume that, to

a first approximation, $K' \approx c_{66}$. Replacing the correct expression for R_a and focusing on the dependence on N_p , N_v , and f_0 we can conclude that for the critical current of a vortex polycrystal, the following relations hold:

$$J_c \propto \begin{cases} f_0^2 (N_p / N_v) & \text{individual GB pinning,} \\ f_0 (N_p / N_v)^{1/2} K (N_v) / N_v & \text{collective GB pinning,} \end{cases} \quad (9)$$

respectively, for low and high defect concentrations. In Eq. (9) we have exploited the identity

$$B = \Phi_0 n_v, \quad (10)$$

and the relation

$$c_{66} \approx \frac{\Phi_0 B}{(8 \pi \lambda)^2}, \quad (11)$$

which holds within the range of vortex densities explored here.¹ Furthermore, the dependence of the vortex lattice constant a on the magnetic induction has been taken into account,¹ as in

$$a = \left(\frac{2}{\sqrt{3}} \right)^{1/2} \left(\frac{\Phi_0}{B} \right)^{1/2}, \quad (12)$$

so that both b and D are proportional to $1/\sqrt{n_v}$. It is also implicit in Eq. (9) that the critical current J_c is proportional to the 2D critical force $b \sigma_c$. We can now compare our theoretical predictions of grain-boundary pinning to our numerical results for FC driven vortex polycrystals. Figure 1 shows how, for low defect concentrations, critical currents grow linearly with N_p , while for higher pinning densities, a square-root growth of the critical current J_c describes the response of the system appropriately within the provided error bars. In order to assess the agreement of the square-root law quantitatively, we performed a nonlinear fit of the data in the collective pinning region with an iterative regression algorithm. Results are shown in Fig. 5, where evidence of sublinear growth is provided and an exponent very close to 1/2 is found. The agreement with the theory is thus remarkable.

A further argument in favor of the GB-pinning picture is provided by the connection between critical currents and grain sizes. GB-pinning theory predicts that the typical grain size R_g in a relaxed configuration should follow the relation $R_g \propto 1/\sigma_c$.^{28,29} If GB depinning truly is the mechanism that drives the threshold dynamics of a vortex polycrystal, one should be able to observe that connection. Indeed, we mentioned above that in the individual GB-pinning region, where critical currents increase linearly upon increasing the defect density, grain sizes are found to decrease rapidly. On the other hand, in the collective pinning region, where both theory and simulations suggest that critical currents exhibit a square-root growth, the decrease in grain sizes slows down. A quantitative estimate of grain sizes in simulations would further corroborate this picture, although this might be a challenging task in the collective pinning regime, due to the discrete nature of the system and the limited grain sizes involved. In order to address these issues, we are currently

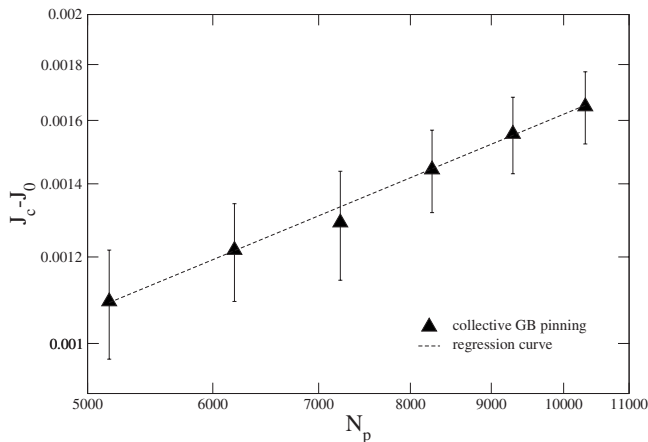


FIG. 5. Iterative nonlinear regression curve for the expected values of the critical current J_c as a function of the number of pinning points N_p . Logarithmic scales are used in both axes. Here J_0 is a fitting parameter. We found $J_c - J_0 \propto N_p^{0.59}$. This result confirms the prediction of sublinear growth. Moreover, the agreement with the expected square-root behavior (see text) is significant and the small deviation is possibly due to the limited number of points and the restricted range of available values.

working on the analysis of diffraction patterns and real-space deformation fields and our findings will be the subject of a future publication.

At this point, we should note that in our simulations grain boundaries develop spontaneously during the relaxation process. The fact that the global behavior matches the one analytically predicted for a GB-pinning dominated system allows us to conclude that GB pinning is the relevant mechanism that drives vortex polycrystal depinning and produces critical-current anomalies, such those observed in experiments. The first equation in Eq. (9) also allows a prediction of the dependence of J_c on the magnetic field $H \propto N_v$, for the case of low pinning density. Our theory suggests $J_c \propto 1/N_v$. Indeed, Fig. 2 shows that our numerical results appear in good agreement with that prediction. Experimental curves of J_c vs H for FC samples qualitatively confirm that behavior, for relatively low fields, far enough from the peak-effect region.^{2,8} However, to our knowledge, no quantitative data are available at present. This would represent an interesting experimental test of our prediction, together with a study of the J_c vs H relation in the collective pinning regime. This would unveil the physics hidden behind the $K(N_v)$ function in Eq. (9) and ultimately allow a deeper understanding of how a complex GB network statistically affects mechanical properties of a vortex lattice.

In the light of the above observations, we can infer that plastic flow in vortex polycrystals is dominated by the glid-

ing motion of dislocation assemblies such as grain boundaries, in analogy with nanocrystalline materials. A typical fingerprint that corroborates our view is the experimental observation of broadband noise spectra in dc-driven vortex arrays.³⁰ Such a feature, also known as $1/f$ noise, is a natural consequence of the collective dynamics of dislocation assemblies,³¹ as opposed to the washboard-frequency peaks, which commonly encompass the periodicity of a dislocation-free lattice. Indeed, by means of Delaunay triangulations we observe that in our simulations, right above depinning, dislocations are created and annihilated at the same rate. At higher drives, in agreement with experiments, healing takes place in the form of a recrystallization process. After healing, by lowering the applied current the hysteresis cycle is recovered.⁶ Current annealing is more effective for higher vortex densities, i.e., stiffer vortex arrays, hence the steady flow of a dense polycrystalline vortex array along the driving direction eventually resembles the flow response of a perfect vortex crystal. On the contrary, less dense or softer arrays remain topologically defected for all the time span of the numerical simulations.

In conclusion we performed a numerical study of plastic depinning in field-cooled vortex lattices. We observed the emergence of dislocation assemblies such as grain boundaries and investigated their role in vortex dynamics. Critical currents are found to follow the laws that we predicted analytically for grain-boundary depinning processes. Grain-boundary depinning thus proves the relevant mechanism accounting for the response of such systems. Our theory of GB depinning is able to explain several experimental observations such as the spatial heterogeneity of the system at the threshold, the high-drive annealing of the FC state, the emergence of memory effects, and the appearance of broadband voltage noise. We established a tight connection between the topology of the vortex polycrystal and its response to externally applied currents and explored the dependence of critical currents and velocities on the density of impurities. Recent experiments on colloidal polycrystals have partially studied this dependence and provided results that agree with the predictions of our model.²⁷ We would like to propose a more systematic analysis in the same direction.

We acknowledge fruitful discussions with A. Kolton, M. Zaiser, and S. Zapperi. This work was financially supported by the Ministerio de Educación y Ciencia (Spain), under Grant No. FIS2007-66485-C02-02. M.C.M. also acknowledges the Generalitat de Catalunya (*Distinció and Programa I3*) and the Ministerio de Educación y Ciencia (*Programa I3*) for additional financial support. P.M. acknowledges funding from the European Social Fund through the Juan de la Cierva Programme.

- ¹G. Blatter, M. V. Feigel'man, V. B. Geshkenbein, A. I. Larkin, and V. M. Vinokur, *Rev. Mod. Phys.* **66**, 1125 (1994).
- ²W. Henderson, E. Y. Andrei, M. J. Higgins, and S. Bhattacharya, *Phys. Rev. Lett.* **77**, 2077 (1996).
- ³Z. L. Xiao, E. Y. Andrei, P. Shuk, and M. Greenblatt, *Phys. Rev. Lett.* **85**, 3265 (2000); Z. L. Xiao, E. Y. Andrei, P. Shuk, and M. Greenblatt, *Phys. Rev. Lett.* **86**, 2431 (2001).
- ⁴A. Pautrat, J. Scola, Ch. Simon, P. Mathieu, A. Brulet, C. Goupil, M. J. Higgins, and S. Bhattacharya, *Phys. Rev. B* **71**, 064517 (2005).
- ⁵B. Sas, F. Portier, K. Vad, B. Keszeti, L. F. Kiss, N. Hegman, I. Puha, S. Mészáros, and F. I. B. Williams, *Phys. Rev. B* **61**, 9118 (2000).
- ⁶P. Moretti, M. Carmen Miguel, and S. Zapperi, *Phys. Rev. B* **72**, 014505 (2005).
- ⁷P. Le Doussal, M. C. Marchetti, and K. J. Wiese, *Phys. Rev. B* **78**, 224201 (2008).
- ⁸R. Wördenweber, P. H. Kes, and C. C. Tsuei, *Phys. Rev. B* **33**, 3172 (1986).
- ⁹W. Henderson, E. Y. Andrei, and M. J. Higgins, *Phys. Rev. Lett.* **81**, 2352 (1998).
- ¹⁰Y. Paltiel, E. Zeldov, Y. N. Myasoedov, H. Shtrikman, S. Bhattacharya, M. J. Higgins, Z. L. Xiao, E. Y. Andrei, P. L. Gammel, and D. J. Bishop, *Nature (London)* **403**, 398 (2000).
- ¹¹M. Marchevsky, M. J. Higgins, and S. Bhattacharya, *Phys. Rev. Lett.* **88**, 087002 (2002).
- ¹²I. V. Grigorieva, *Sov. Phys. JETP* **69**, 194 (1989).
- ¹³I. V. Grigorieva, *Supercond. Sci. Technol.* **7**, 161 (1994).
- ¹⁴M. V. Marchevsky, Ph.D. thesis, Leiden University, 1997.
- ¹⁵M. V. Marchevsky, A. Keurentjes, J. Aarts, and P. H. Kes, *Phys. Rev. B* **57**, 6061 (1998).
- ¹⁶F. Pardo, F. De La Cruz, P. L. Gammel, C. S. Oglesby, E. Bucher, B. Batlogg, and D. J. Bishop, *Phys. Rev. Lett.* **78**, 4633 (1997).
- ¹⁷Y. Fasano, M. Menghini, F. de la Cruz, Y. Paltiel, Y. Myasoedov, E. Zeldov, M. J. Higgins, and S. Bhattacharya, *Phys. Rev. B* **66**, 020512(R) (2002).
- ¹⁸H. Dai, J. Liu, and C. M. Lieber, *Phys. Rev. Lett.* **72**, 748 (1994).
- ¹⁹J. A. Herbsommer, G. Nieva, and J. Luzuriaga, *Phys. Rev. B* **62**, 678 (2000).
- ²⁰M. C. Faleski, M. C. Marchetti, and A. A. Middleton, *Phys. Rev. B* **54**, 12427 (1996).
- ²¹M. Chandran, R. T. Scalettar, and G. T. Zimányi, *Phys. Rev. Lett.* **89**, 187001 (2002).
- ²²Such a length is in fact fine-tuned in the x and y directions, in order to allow an ideal triangular vortex lattice to fit in the simulation box.
- ²³P.-G. de Gennes, *Superconductivity of Metals and Alloys* (Benjamin, New York, 1966).
- ²⁴Current densities are measured in units of $c\Phi_0/(8\pi^2\lambda^3)$, as in Ref. 6.
- ²⁵T. Klein, I. Joumard, S. Blanchard, J. Marcus, R. Cubitt, T. Giamarchi, and P. Le Doussal, *Nature (London)* **413**, 404 (2001).
- ²⁶H. J. Jensen, A. Brass, Y. Brechet, and A. J. Berlinsky, *Phys. Rev. B* **38**, 9235 (1988).
- ²⁷A. Pertsinidis and X. S. Ling, *Phys. Rev. Lett.* **100**, 028303 (2008).
- ²⁸P. Moretti, M. Carmen Miguel, M. Zaiser, and S. Zapperi, *Phys. Rev. B* **69**, 214103 (2004).
- ²⁹P. Moretti, M. Carmen Miguel, M. Zaiser, and S. Zapperi, *Phys. Rev. Lett.* **92**, 257004 (2004).
- ³⁰Y. Togawa, R. Abiru, K. Iwaya, H. Kitano, and A. Maeda, *Phys. Rev. Lett.* **85**, 3716 (2000).
- ³¹L. Laurson and M. J. Alava, *Phys. Rev. E* **74**, 066106 (2006).